International Journal of Heat and Mass Transfer 146 (2020) 118804

Contents lists available at ScienceDirect

International Journal of Heat and Mass Transfer

journal homepage: www.elsevier.com/locate/ijhmt

The stagnation point heat transfer under partially-developed submerged jets

Barak Kashi, Herman D. Haustein *

School of Mechanical Engineering, Faculty of Engineering, Tel Aviv University, Tel Aviv, Israel

ARTICLE INFO

Article history:
Received 18 August 2019
Received in revised form 26 September 2019
Accepted 27 September 2019

Keywords:
Submerged jet impingement
Stagnation flow
Heat transfer
Wall influence

ABSTRACT

Laminar jet impingement is an efficient method for heat transfer processes, though much of its hydrodynamics and the resulting convection are still not fully understood. As previously shown, stagnation-point heat transfer (Nu_0) depends directly on the near-axis radial acceleration (A_0) varying strongly with nozzle diameter (d), normalized nozzle length (L), normalized nozzle-to-plate spacing (H) and flow rate (Re), therefore a general expression is here developed for this key parameter.

Through streamline-bending analysis it was identified that A_0 can be derived from the characteristics of the velocity profile arriving at the point of transition from free jet flight to stagnation flow (at z_w). This analysis also led to the identification of the curvature of the velocity profile in the jet-core as the key factor dictating A_0, over a domain defined by a new characteristic scale R_c. Examination of this curvature, resolves the apparently contradicting trends in the literature for A_0's dependence on flight distance. Moreover, it explains the occurrence of maximal heat transfer, when h is set around the potential core length.

Building on the theoretical analysis, an explicit, yet universal, model for Nu_0 was developed in terms of nominal geometry and flow rate, rather than relying on the often-unknown arrival profile, and validated against simulations over a wide range of conditions ($0.003 \leq L$, $0.001 \leq H$, $250 \leq Re \leq 2000$). Therein, this model pin-points the location of the maximal heat transfer for any issuing profile, enabling efficient design and optimization.

Finally, identifying z_w as the stagnation-flow characteristic scale instead of d, enabled extension of an existing wall-approach model to include partially-developed profiles and longer flights. Then requiring the model's conformity to previous theory gave an explicit expression for z_w – the lower-bound of $H{\cdot}Re$ still permitting heat transfer analysis assuming decoupling between the nozzle and wall flows.

1. Introduction

Laminar jet impingement has many applications related to heat and mass transfer in drying and cooling processes, while many of its underlying hydrodynamic aspects are still not clear. For cooling applications the convective heat transfer is subject to this canonical, though intricate, flow field [2,3]. Besides these applications, jet flow is often employed as a measurement tool for cell adhesion [4,5], erosion, coating and particulate material removal for cleaning or detection purposes [6–8], giving rise to the importance of describing also the wall pressure and shear stresses. Beyond the applications, many more fundamental aspects of the hydrodynamics are still being studied [9,10], which will benefit greatly from clarification of the basic laminar flow, inherent phenomena and resulting transport, undertaken here.

Submerged jet impingement can be described as having multiple distinctly different stages, depicted in Fig. 1. Initially, it emerges from a nozzle with a specific issuing profile that depends on the nozzle shape and length [11]. If that profile is partially uniform, it will exhibit a potential-core, within which the axial centerline velocity w_C remains constant and unaffected, due to negligible velocity gradients near the axis, over a limited distance (the potential core length). Beyond the potential core, the velocity profile continues to develop and interact with the surrounding stagnant liquid, and eventually a state of profile self-similarity is reached [12]. During any of the aforementioned stages, the jet may begin to approach the impingement surface, transitioning from a free-jet to stagnation-flow. Beginning at a distance denoted z_w – the height of the stagnation zone, where it begins to significantly decelerate axially and accelerate radially, i.e., deflect as a result

* Corresponding author.
E-mail address: hermanh@tauex.tau.ac.il (H.D. Haustein).

https://doi.org/10.1016/j.ijheatmasstransfer.2019.118804
0017-9310/

Nomenclature

A	wall-flow radial acceleration, normalized by nozzle diameter and mean axial velocity [−]
c	fraction of the centerline velocity [−]
C	mean radial-velocity contribution to the vorticity in the stagnation flow [−]
C_1	model constant [−]
d	nozzle diameter [m]
h	nozzle-to-heater spacing, normalized by nozzle diameter [−]
H	nozzle-to-heater spacing, normalized by nozzle diameter and Reynolds number [−]
l	nozzle length, normalized by nozzle diameter [−]
L	nozzle length, normalized by nozzle diameter and Reynolds number [−]
M	momentum flux, normalized by that of a uniform profile jet [−]
p	local pressure at the boundary layer edge, normalized by centerline dynamic pressure at the onset of wall influence [−]
r	wall-flow radial coordinate, normalized by nozzle diameter [−]
r_j	radial extent of the arriving jet, normalized by nozzle diameter [−]
R	free-jet flight radial coordinate, normalized by nozzle diameter [−]
R_c	jet-core characteristic radius, normalized by nozzle diameter [−]
S_1	half the arriving velocity profile's near-axis curvature, normalized by the centerline velocity and the nozzle diameter squared [−]
t	time [s]
u	radial velocity component, normalized by the mean axial velocity [−]
w	axial velocity component, normalized by the mean axial velocity [−]
x	flight axial coordinate, measured from the nozzle exit plane and normalized by nozzle diameter [−]
ΔX	virtual origin length, normalized by nozzle diameter and Reynolds number [−]
z	wall-flow axial coordinate, measured from the wall and normalized by nozzle diameter [−]
Nu	Nusselt number, based on nozzle diameter [−]
Pr	Prandtl number of the fluid [−]
Re	Reynolds number, based on nozzle diameter and mean axial velocity [−]

Greek symbols

α	thermal diffusivity [m^2/s]
δ	boundary layer thickness at the stagnation point, normalized by nozzle diameter [−]
δ_0^*	displacement thickness of the stagnation point boundary layer, normalized by nozzle diameter [−]
$\delta_{0,n}$	displacement thickness of the flow issuing from the nozzle, normalized by nozzle diameter [−]
λ	fitting constant in a previous model by Bergthorson *et al.* [1] [−]
ν	kinematic viscosity [m^2/s]
ρ	density [kg/m^3]
ζ	wall-approach coordinate, normalized by stagnation zone height [−]

Subscripts

c	at the centreline or within the core
dev	fully developed profile
f	final
i	initial
j	of the jet
max	maximal value
n	at the nozzle
par1	partially developed profile issuing from a pipe-type nozzle of $L = 0.0015$
par2	partially developed profile issuing from a pipe-type nozzle of $L = 0.003$
par3	partially developed profile issuing from a pipe-type nozzle of $L = 0.006$
par4	partially developed profile issuing from a pipe-type nozzle of $L = 0.01$
par5	partially developed profile issuing from a pipe-type nozzle of $L = 0.014$
pc	potential core
uni	uniform profile
w	at the onset of wall influence $z = z_w$
0	at the stagnation point

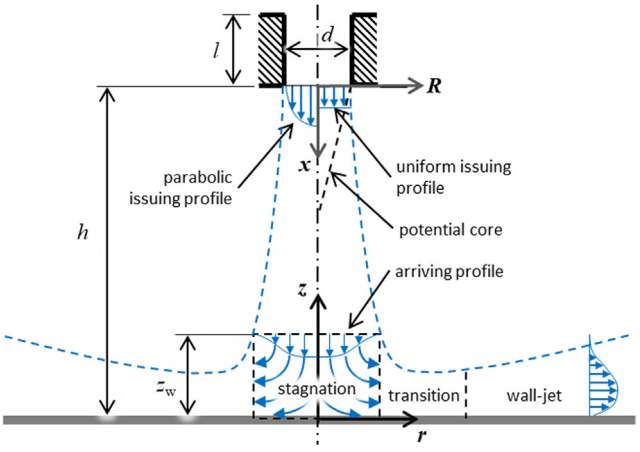

Fig. 1. Schematic diagram of the impinging jet problem with definition of flow zones.

of the stagnation-point pressure buildup. Within this zone, a classic solution claims self-similar radial velocity profiles characterized by linear acceleration outward from the stagnation point [13]. As the flow progresses in the radial direction, this acceleration is overtaken by the radially growing cross-section area, and thus deceleration begins. The zone of the free-stream velocity maximum and initial deceleration is denoted the transition zone, which is followed by the developed wall-jet zone, where profile full self-similarity is recovered [14].

The problem of jet-flight, prior to reaching impingement zone, has been dealt with extensively [15–17]. A recent work by the authors showed that the arriving profile can be predicted for a wide range of conditions, both near the nozzle or at intermediate flight distances and beyond, provided that the issuing profile is known [17]. For this reason, the present study assumes that the jet profile, arriving at the stagnation zone height ($z = z_w$), is known – similarly to a previous study [18]). This assumption is later relaxed and a new model for finding the required arriving profile characteristics is developed. As the present study deals with the

flow's wall interaction it focuses on the region near the stagnation point and considers primarily the jet's near-axis characteristics upon arrival at the stagnation zone height (z_w). Therein, a rather detailed review of existing theory is given, to emphasis the remaining gap in prediction and to elaborate the existing foundation for the extension obtained by the present theoretical analysis.

The approaching flow just begins to be influenced by the wall and static pressure begins to rise at the uppermost point of the stagnation zone – here termed z_w. From there the flow undergoes deceleration up to standstill at the stagnation point, through a process termed the wall approach. Though a few previous studies of wall approach exist [1,19,20], only [20] attempted to define a quantitative criterion for the *onset of wall influence*, i.e., the location of z_w (there termed the "plate distance") which determines *the stagnation zone height*. That criterion relied on the shift of balance within the axial momentum equation – which can in general be found only from scrutiny of simulation. Furthermore, it was only tested on the case of fully-developed issuing jets, first in the free-surface configuration (Rohlfs, C. Ehrenpreis, et al. 2014), and later in the submerged case as well [22]. A new simple alternative to this criterion is here proposed, which is based on the nominal problem parameters and found to be valid for all issuing profiles in the submerged configuration.

Beyond the onset, the deceleration towards the wall for quasi-uniform (turbulent) jet's impingement was studied by Kostiuk *et al.* [23]. The empirical model he suggested for deceleration on the axis, was later modified by Bergthorson *et al.* [1] for laminar flows, giving

$$\frac{w_c}{w_{c,w}} = \mathrm{erf}\left(\lambda\left(z-\delta_0^*\right)\right) = \mathrm{erf}\left(\lambda\left(z-\frac{0.755}{\sqrt{Re\,A_0}}\right)\right) \tag{1}$$

where, $w_{c,zw}$ is the centerline velocity upon arrival, z the axial coordinate normalized by jet diameter and δ_0^* is the displacement thickness of the boundary layer flow at the stagnation point (indicated by subscript 0) – with a value around one-third of the boundary layer, it is generally negligible for high-Re conditions. In addition, the constant λ was shown to have a weak dependence on Reynolds number, though not on profile, ranging in value from 2.21 to 1.88 for $400 \le Re \le 1400$. They later suggested normalizing (z-δ_0^*) by the displacement thickness of the flow issuing from the nozzle $\delta_{0,n}$. However, this choice of normalization is only justifiable for the short flights examined there [1] – as with significant velocity profile relaxation the nozzle's effect fades. More relevantly, here an alternative normalization by the stagnation zone height (z_w) is examined, dependent not on the *nozzle* conditions but rather on the characteristics of the *arriving* profile. Furthermore, this height (z_w) is the lower bound for nozzle-to-wall spacing below which significant flow interaction occurs and an entirely different regime is encountered. Therefore, previous heat transfer correlations have been limited to $h > 2d$ [24,25], though here the limit is expressed through the problem parameters.

Within the stagnation zone, in the near-wall region the classic solution by Homann [13], assumes the inviscid free-stream velocity is known and derives the boundary layer velocity distribution from it. Therein, this solution assumes a uniform incoming flow and a constant free-stream radial velocity gradient $A \equiv \mathrm{d}u/\mathrm{d}r$, where u is the radial velocity normalized by the average arriving jet (axial) velocity w_m and r is the radial coordinate normalized by jet diameter d. This classical numerical solution is available in tabulated form [12], and has recently been approximated in continuous form by the authors [26]. It gives the key flow aspects as:

$$u = A_0 \cdot r \tag{2}$$

$$w = -2A_0\, z \tag{3}$$

$$\delta = \frac{1.95}{\sqrt{A_0 \cdot Re}} \tag{4}$$

$$p_H(r)|_{z=\delta} = 1 - \left(\frac{A_0^2}{w_{c,w}^2} r^2\right) \tag{5}$$

where the velocity components are given in the free-stream outside the boundary layer, except $w_{c,w}$ which is the centerline axial velocity upon the onset of wall-approach, δ is the boundary layer thickness normalized by d, and Re is the Reynolds number defined by jet diameter and average issuing velocity ($Re = \mathrm{d}w_m/\nu$). In addition, p is the pressure at the edge of the boundary layer following Bernoulli's law and normalized by $\frac{1}{2}\rho w_{c,w}^2$, ρ being fluid density and subscripts c and H indicate the centerline value and Homann's solution accordingly. Note the importance of the radial velocity gradient A_0, further exemplified through the Reynolds-analogy type analysis in Schlichting [12], later adapted for jets by Liu et al. [27] stating that also the stagnation-point heat transfer depends on it:

$$Nu_0 = \sqrt{2A_0 Re}\, G(Pr) \tag{6}$$

where the subscript 0 indicates the stagnation point and the Prandtl number ($Pr = \nu/\alpha$) dependence is approximated there by

$$G(Pr) = \begin{cases} \frac{\sqrt{2Pr/\pi}}{1+0.50455\sqrt{2Pr/\pi}} & Pr < 0.15 \\ 0.53898 Pr^{0.4} & 0.15 \leqslant Pr \leqslant 3 \\ 0.60105 Pr^{1/3} - 0.050848 & Pr > 3 \end{cases} \tag{7}$$

As the previous equations show, the foundational parameter is A_0, for which values from the literature are plotted against jet flight distance in Fig. 2. As the figure shows, well-known values of A_0 vary significantly between arriving profiles (dependent on both development level and flight distance, H) and also between studies: for an ideal uniform profile $A_0 = 0.743$–0.916 (see Table 1 in Liu et al. (1993)), while for a purely parabolic profile the numerical values of Law and Masllyah [28] ($Re = 1900$ and $h = 2$–4) ranging $A_0 = 3.88$–3.94, are somewhat lower than $A_0 = 4.64$ from a theoretical analysis for jet-near-wall conditions $h < 1$ [29]. In addition to these values, a correlation for A_0 (dash-dot line) is derived from

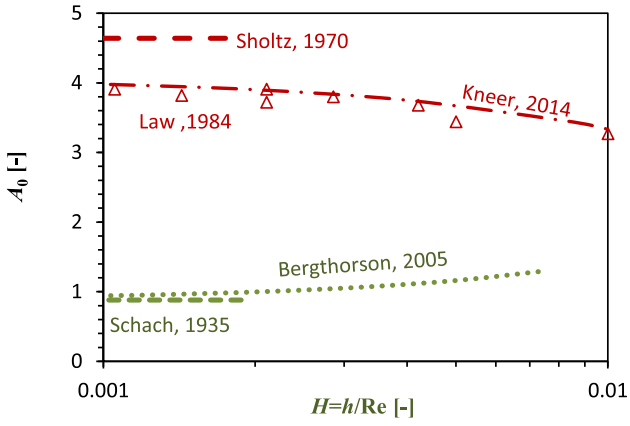

Fig. 2. Dependence of A_0 on issuing profile and flight distance compared to predictions according to two models for the uniform (green) and developed (red) issuing profiles, as well as other values from the literature (see table in Liu et al. [27] with proceeding corrections (Corrections to the values in this table are posted on Prof. Lienhard's MIT webpage: http://web.mit.edu/lienhard/www/stagnation_point_heat_transfer_liquid_jets.pdf (see last page))). (For interpretation of the references to colour in this figure legend, the reader is referred to the web version of this article.)

comparison of the expressions for heat transfer by the authors [22] $Nu_0 \propto w_{c,w}$, while considering classical theory states $Nu_0 \propto \sqrt{A_0}$ [27].

Despite, the importance of this parameter for impingement flow and even more so for heat transfer, values for the entire scope of possible arriving profiles were not found. It is important to note that the arriving profile is a result of both the issuing profile level of development and the level of relaxation during flight, thereby spanning a very wide range of possible profiles [18]. Therefore, rather than just completing the (intermediate) missing data, this parameter's general dependencies are sought.

The present study, with the goal of expressing the flow and resulting heat transfer under all impinging submerged jets, focuses on the free-stream radial velocity gradient. Despite its importance, there is a lack of data and understanding of this gradient $A \equiv du/dr$, and therefore an extensive examination of it is undertaken here. Contrary to Homann's approach, the near-axis (constant) value of A is not assumed to be known, and rather it is derived and its dependencies on the problem parameters are found. In other words, Homann's solution assumed constant acceleration under a **uniform** arriving profile and used a Bernoulli-type relation to find the pressure distribution dictated by it, whereas here a *general* approach is taken – seeking the true pressure distribution and allowing it to dictate the radial acceleration for **all** profiles. This poses the problem of finding a universal conversion of the *dynamic* pressure of the arrival velocity profile to the *static* wall pressure distribution. Resolving this issue reveals the inherent coupling between the incoming axial flow and the outgoing radial one, through the build-up and relaxation of the stagnation pressure.

In effect, the present study deals with the near-axis "stagnation point" (A_0), while a follow-up study is underway to extend these findings to the radial distribution of the flow and heat transfer as well. It will be shown that this new approach allows a more physically correct description of the flow field and wall transport, while covering all arriving profiles.

2. Methods

In the present study meaningful relations between the key jet impingement characteristics are sought in order to relate the known arriving jet parameters to the resulting stagnation-point heat transfer. Firstly, new mathematical relations are derived for the unique case of a fully developed jet. This lays the foundation for dealing with partially-developed profiles, especially those which have a *local* non-negligible curvature at the axis, i.e., that do not have a potential core. Subsequently, the unique *global* curvature of each profile is defined, enabling a general description for all profiles, including those with a potential core. While these new derivation are applicable when the arriving profile is known, an approximate model is also developed in nominal terms of geometry and flow rate. All stages of derivation and their new predictions are evaluated against a wide range of numerical simulations.

2.1. Stagnation-point heat transfer analysis

In order to provide the wall-pressure distribution the streamline bending is first analysed. This is based on the premise that the static pressure at each radial location near the wall (r at the edge of the boundary layer δ) has a corresponding location with an equal dynamic pressure in the arrival profile (R at the top of the stagnation zone z_w). The entire analysis and derivation are given in appendix A, and lead to the relation:

$$r \equiv r|_{z=\delta} = \sqrt{R^2\Big|_{z=z_w} - 8C^2 z_w^2 \ln\left(\frac{w(R)}{w_c}\Big|_{z=z_w}\right)} \tag{8}$$

During the derivation, a single unknown scaling parameter emerged C, representing the fraction of vorticity passed over from the primary source to the secondary one, $\partial u/\partial z = C^2 \cdot \partial w/\partial r$. This characteristic ratio changes from $C = 0$ in developed pipe-type nozzle flow, through $C \propto 1/\sqrt{Re}$ during flight and increases towards $C \sim 1$ within the stagnation zone, its mean value will be estimated in the following. This new relation is equivalent to a remapping of the dynamic pressure, contained within the arrival "*contracted*" (R-dependent) velocity profile, along the bent streamlines to the static pressure at the wall in the "*standard*" radial coordinate r. In other words, the dimensionless pressure distribution on the wall can be found from the known arriving velocity profile according to Bernoulli's law along the streamlines, bending as they go from z_w down to δ:

$$p(r) = \frac{\frac{1}{2}\rho w_w^2(R(r))}{\frac{1}{2}\rho w_{c,w}^2} \tag{9}$$

As the analysis follows the flow direction from the known arrival conditions streamwise towards the wall, an explicit relation for $R = R(r)$ is required, rather than the inverse one given by Eq. (8). First, the *unique* case of a purely parabolic arriving profile is seen to deliver a simple explicit relation, which is then followed by a *general* procedure for all other profiles based on a near-axis expansion-series of the arrival velocity profile.

For the specific case of a pure parabolic profile (subscript dev) arriving at z_w, a *two-way* explicit relation exists between R and r, which uses the primary branch of the Lambert-W function and allows the expression of the wall pressure as a function of the standard radial coordinate (r) instead of R:

$$p_{dev}(r) = \left(\frac{1}{4} - 8\,C^2 z_w^2 \mathrm{LambertW}\left(\frac{e^{\frac{1-4r^2}{32C^2 z_w^2}}}{32C^2 z_w^2}\right)\right)^2 \tag{10}$$

Requiring that this pressure distribution around the axis complies with that of Homann (Eq. (5)) leads to a relation between A_0, C and z_w for this limiting case:

$$A_{0,dev} = \sqrt{\frac{1}{C^2 z_w^2 + 1/32}} \tag{11}$$

The value found by present simulation for this limiting case ($A_{0,dev} \cong 4.33$ for conditions of $z_w \cong 1$, as claimed in Kneer et al. [22])) is seen to be centered within previous results: $A_{0,dev} = 4.64$ found for $h < z_w$ in the rather complex analysis of Scholtz and Trass [30] and $A_{0,dev} = 3.94$ for $h = 2$ in the experimental data of Law [28]. Following previous pressure distribution results for $h < 1$ (Fig. 9 in Bergthorson et. al. [1]), it is reasonable to deduce that the high value of $A_{0,dev} = 4.64$ is due to significant nozzle-wall flow interaction (found for $h = 0.25$ there). Therefore it is not representative of the impingement of the purely parabolic profile dealt with here. Using the value found by present simulation in Eq. together with $z_w \cong 1$, (reported by Kneer et al. [22]) leads to $C^2 \cong 0.022$. According to the derivation of Eq. in the Appendix, the value of this constant fixes the integral contribution to streamline bending of the *normalized* incoming velocity gradient $(\partial w/\partial r)(r/w)$ and the *normalized* stagnation zone height (z_w/r), it is therefore taken as *common* to all profiles. Finding this constant lays the foundation for generalizing the streamline bending analysis and pressure distribution description, and is supported by the full numerical solutions for multiple representative profiles.

Proceeding to the general analysis of wall pressure distribution suitable for all arriving profiles, it is seen that the profiles are usually not given by simple exact functions, such as the purely parabolic profile, and need to be approximated [17]. Nonetheless, as the present study is primarily concerned with the near-axis

conditions, all profiles without a potential core can still be approximated by a parabolic-like approximation. The expansion of the arrival profile around the axis is:

$$w = 1 + S_1 R^2 + \mathrm{O}\left(R^4\right) \tag{12}$$

where S_1 is half the profile curvature at the axis, $S_1 \equiv \frac{1}{2}\,\partial^2 w/\partial r^2$. This expansion provides us with the required invertible relation needed in Eq. (9), so that near the axis the dependence of R on r can now be written as

$$\lim_{R\to 0}\left(\frac{r}{R}\right)^2 = \left(1 - 8C^2 z_w^2 S_1\right). \tag{13}$$

Introducing this limit together with the near-axis profile expansion (Eq. (12)) into Eq. (9) and expanding it as a Maclaurin-series of a small term ($r \to 0$), gives the near-axis wall pressure at leading order

$$p(r)|_{r\to 0} = 1 + 2S_1\left(\frac{r^2}{1 - 8C^2 z_w^2 S_1}\right) + \mathrm{O}(r^4) \tag{14}$$

Requiring now that this near-axis pressure converges to Homann's solution (Eq. (4) must be valid there), dictates a constraint on the curvature at the axis, denoted $2S_1$. This constraint, together with the value of C found previously and assumed common to all profiles, directly leads to a new relation for A_0:

$$A_0 = \sqrt{\frac{2S_1 w_{c,w}^2}{8\,C^2 z_w^2\,S_1 - 1}} \tag{15}$$

The importance of the arriving profile's curvature ($2S_1$) to the resulting stagnation-point radial-acceleration is here identified for the first time. Practically, this curvature can be uniquely found for partially-developed profiles if Eq. (12) is fitted to them over the jet's core domain – here defined as $0 < r < r_j/6$ (where r_j is the arriving jet's total radial extent, defined by a cut-off at 5% of the centerline velocity).

Eq. (15) is an asymptotic relation derived under the assumptions that the incoming profile is sufficiently described by the leading-order expansion of Eq. (12), but this breaks down when $S_1 \to 0$.

As a significant part of the parametric space considered here contains the jet potential cores, where the near-axis curvature S_1 is negligible, a more general form than Eq. (15) is sought. Therefore, focusing on the limit of very small S_1, the second term in the denominator is seen to be negligible for $|S_1| \le \frac{1}{2}\,1/z_w^2$, conveniently also circumventing the need to deal with the stagnation zone height (z_w) during this analytical effort. Nonetheless, this important parameter, for which a general description is still lacking, is empirically dealt with in Appendix B.

Proceeding under the requirement of $|S_1| \le \frac{1}{2}\cdot 1/z_w^2$, with the much-simplified form for A_0:

$$A_0|_{|2S_1|\le 1/z_w^2} \cong \sqrt{-2\,S_1 w_{c,w}^2} \tag{16}$$

It is now recognized that S_1, being half the profile curvature normalized by the centerline velocity, can be written as a second-order derivative in finite-difference terms near the axis:

$$\lim_{r\to 0}\sqrt{-2\,S_1 w_{c,w}^2} = \sqrt{-2\left[\frac{1}{2}\,\frac{2\Delta w_w/w_{c,w}}{\Delta R^2}\right] w_{c,w}^2} \propto \sqrt{-2\,\frac{1-c}{R_c^2}\,w_{c,w}^2} \tag{17}$$

where the square brackets are S_1 in finite-difference terms, and c is a fraction of the centerline velocity corresponding to the location of R_c (see Fig. 3). Therein, in order to cover the entire range of relevant arrival profiles, two concessions were made: at high issuing

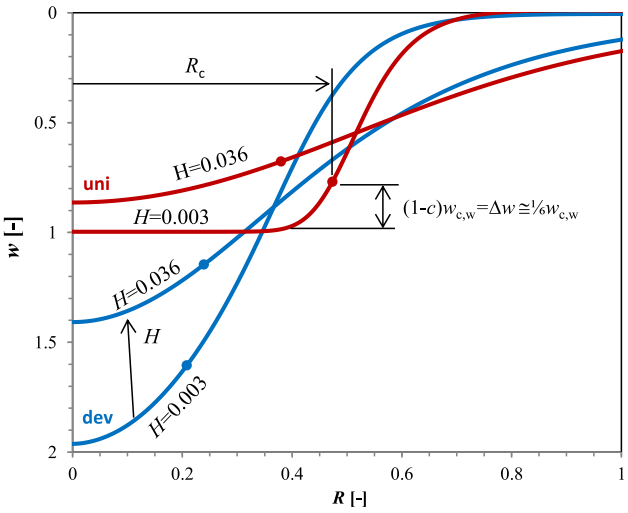

Fig. 3. Various arriving velocity profiles from the flight of extreme issuing profiles. Note the core extent (dot on the lines) defined by R_c and c and profile's shape relaxation with flight distance H.

curvatures this simplified form is no longer required to converge back to the previous solution (Eq. (15)) and an additional constant C_1 is introduced in order to comply even with extreme values. Moreover, the known extreme values of $A_{0,uni}$ and $A_{0,dev}$, determine both $C_1 = A_{0,uni}/\sqrt{24}$ and $c \cong 5/6$, resulting in the following explicit form:

$$A_0 = C_1\,\frac{\sqrt{1-c}}{R_c}\,w_{c,w} = \frac{A_{0,uni}}{2}\,\frac{w_{c,w}}{R_c} = 0.44\,\frac{w_{c,w}}{R_c} \tag{18}$$

In other words, R_c is a new scale representing the effective curvature of the jet core (and not just at the axis) for all profiles and is found on the arrival profile as the radial distance where the axial velocity is equal $c\cdot w_{c,w}$ or where $w(R_c) \cong w_{c,w}\cdot 5/6$, as indicated for several profiles in Fig. 3.

With A_0 given by this simple expression the heat transfer is effectively solved (according to Eq. (6)), provided that the arriving profile is fully known. However, as this is mostly not the case and as the arrival profile is a culmination of both the flow's development in the pipe and subsequent relaxation during flight, a new description for A_0 directly relating it to known parameters is formulated hereafter.

It is interesting to note that the maximal radial acceleration $A_{0,dev}$, found here through simulations, corresponds to a **maximal heat transfer** that can be expected under a submerged laminar jet issuing from a pipe-type nozzle: $Nu_{0,max}/(G(Pr)\cdot Re^{1/2}) = (2\,A_{0,dev})^{1/2} \cong 2.943$. This value is slightly higher than empirical correlations recently developed by one of the authors, based on extensive numerical simulations of a fully-developed issuing profile, where $Nu_{0,max} = 2.82$ and 2.9 for free-surface and submerged jets [22].

2.2. The direct heat transfer description

In the interest of providing a simple explicit expression for the heat transfer $Nu = f(A_0(w_{c,w}/R_c))$ in nominal geometric terms L and H, a model is here developed for the evolution of $w_{c,w}$ and R_c, both inside the nozzle and subsequently during flight. This model follows a consistent methodology of a transition between two analytical or known asymptotes, leaving only the transition to be defined.

First, it is recalled that the evolution of the centerline velocity during jet flight has recently been dealt with extensively by the authors [17,21]. However, both those models employed several empirical elements and neither addressed the newly identified

key locus R_c. It is proposed that the evolution of both $w_{c,w}$ and R_c can be described as an exponential transition from an analytical near-nozzle solution to an analytical quasi-self-similar one far-downstream, with the only degree of freedom being the scale over which the transition occurs.

In the far-downstream limit, modification of Schlichting's self-similar jet by means of a virtual origin has brought it upstream at the far limits of the relevant range, in the form of:

$$w(R,X) = \frac{3}{32}\frac{M(L)}{(X+\Delta X(L))\left(1+\frac{1}{64}\frac{R^2}{(X+\Delta X(L))^2}\right)^2} \tag{19}$$

where the issuing momentum flux, $M(L) = 8\int_0^{1/2} w_n^2(L) R\,dR$, ranges from 1 to 4/3 from uniform to fully developed profiles. Although various values of virtual origin (ΔX) have been proposed [15,16,31], a recent study by the authors identified the maximal permissible value. This analysis brought the self-similar solution closer to the jet nozzle than ever before, subject to the issuing profile's level of development – a direct function of pipe length L [17].

Beyond the known far-downstream solution, the near-nozzle asymptote requires some further analysis. In general, the near-nozzle centerline velocity is given by a leading order MacLaurin-series, i.e., $w(L,X\to 0) = w_n + X\cdot\partial w/\partial X$. The issuing value $w_n = w_n(L)$ has been extensively dealt with in developing pipe-flow studies [32,33], whereas the near-nozzle *gradient* is found through simplification of the steady axial momentum balance during flight, as follows.

Linearizing the axial momentum balance in the limit of $X \to 0$ around the axis ($R \to 0$) as:

$$w\frac{\partial w}{\partial x} \cong w_n\frac{\partial w}{\partial x} = \frac{1}{Re}\frac{1}{R}\frac{\partial}{\partial R}\left(R\frac{\partial w}{\partial R}\right) \cong \frac{2}{Re}\frac{\partial^2 w}{\partial R^2} \tag{20}$$

Or in terms of issuing profile curvature and using $x = X\cdot Re$:

$$\frac{\partial w}{\partial X} \cong 4S_1 \tag{21}$$

and the near-nozzle velocity asymptote becomes:

$$\lim_{X\to 0} w = w_n + 4S_1 X \tag{22}$$

Therefore, the centerline velocity's transition from near-nozzle to far-downstream flight over a finite domain (H), can be written as:

$$\frac{1}{w_{c,w}(L,H)} = \underbrace{\frac{e^{-\left\{\frac{w_{c,n}^2(L)}{w_{c,dev}^2}\right\}\frac{w_{c,uni}}{w_{c,n}(L)}\frac{H}{H_0}}}{w_{c,n}(L)+4S_1(L)H}}_{\text{near asymptote}} + \underbrace{\frac{32}{3}\frac{(H+\Delta X(L))\cdot\left(1-e^{-\left\{\frac{w_{c,n}^2(L)}{w_{c,dev}^2}\right\}\frac{w_{c,uni}}{w_{c,n}(L)}\frac{H}{H_0}}\right)}{M(L)}}_{\text{far asymptote}} \tag{23}$$

As the far-downstream solution tends to infinity at the nozzle, the transition between it and the near-nozzle asymptote must be of an inverse nature, as implemented in the equation. Note that this inverse transition occurs over time (H/w_n) rather than space. Furthermore, this time-scale is profile specific and normalized by the uniform case $H_0/w_{n,uni}$ (where the velocity remains constant $w_{c,uni} = 1$ over the potential core of length $H_0 = H_{pc,uni} \cong 1/60$). Finally, scaling the transition by the jet core momentum flux ($w_{c,n}^2/w_{c,dev}^2$) addresses the delayed convergence to self-similarity of less-developed issuing profiles.

In contrast to $w_{c,w}$, for R_c the far-downstream solution (second term on the RHS in Eq. (24)) becomes very small as the nozzle is approached and a straightforward exponential transition can be employed:

$$R_{c,w}(L,H) = \underbrace{R_{c,n}(L)e^{-\frac{12}{5}\frac{S_1 H}{w_{c,n}}}}_{\text{near asymptote}}\cdot e^{-\frac{H}{H_0}} + \underbrace{16\sqrt{\sqrt{\frac{6}{5}}-1}\left(H+\Delta X(L)\left(1-e^{-H/H_0}\right)\right)}_{\text{far asymptote}} \tag{24}$$

Here again the far-downstream solution is easily obtained by introducing the definition of R_c, $w(R_c) = w_{c,w}\cdot 5/6$ into Schlichting's modified solution and solving for R_c, whereas the near-nozzle asymptote is newly derived hereafter.

Beginning from continuity around the axis ($r \to 0$):

$$\frac{1}{Re}\frac{\partial w}{\partial X} = \frac{\partial w}{\partial x} = -\frac{1}{R}\frac{\partial}{\partial r}(u\cdot R) \underset{R\to 0}{\cong} -2\frac{\partial u}{\partial R} \tag{25}$$

Recalling that within the jet core $\partial w/\partial X \cong 4S_1 = \text{const.}$, the simplified continuity above dictates that the radial velocity in the jet-core must grow linearly from a value of zero at the axis $\partial u/\partial r = \text{const.}$, or

$$4S_1 \cong -2Re\frac{u}{R} = -2Re\frac{1}{R}\frac{\partial R}{\partial t} \tag{26}$$

Converting the time derivative now to a spatial one, using the core axial velocity near the nozzle, w_n (R = Rc):

$$4S_1 \cong -2Re\frac{1}{R}\frac{\partial R}{\partial X}\frac{\partial X}{\partial t} \cong -\frac{2}{R_c}\frac{\partial R_c}{\partial X}w_n|_{R=R_c} \tag{27}$$

Note that on the right hand side of the equation above the analysis has been extended beyond the jet axis to the edge of the core, to R_c, a location around $R = 1/4$, though varying with issuing profile and defined by $w(R_c) = w_{c,w}\cdot 5/6$. Now separating variables and integrating gives

$$\ln\left(\frac{R_c}{R_{c,n}}\right) \cong -\frac{12}{5}\frac{S_1}{w_{c,n}}X \tag{28}$$

Equivalent to an exponential growth of R_c when it issues from the nozzle as:

$$\lim_{X\to 0} R_c = R_{c,n}e^{-\frac{12}{5}\frac{S_1 X}{w_{c,n}}} \tag{29}$$

Giving the near-nozzle asymptote required for its transition to far-downstream behaviour, found to occur over the previously recognized characteristic distance $H_0 = H_{pc,uni} \cong 1/60$.

Evaluation of this new description, including these new asymptotes and the resulting radial acceleration upon impingement, is shown at the beginning of the Results section.

Finally to obtain a fully closed approximate description, key flow characteristics within the *pipe-type nozzle* are required. Several of these characteristics have already been approximated in a previous work of the authors [34], including centerline velocity:

$$\begin{aligned} w_{c,n}(L) &= w_{c,dev} - \left(w_{c,dev} - \underbrace{w_{c,i}}_{=w_n(L_i)}\right)\cdot e^{-\frac{L-L_i}{L_0}} \\ &= 2 - (2-1.389)\cdot e^{-\frac{L-0.003}{1/72}} \end{aligned} \tag{30}$$

While this form was taken directly from the previous work, the values were slightly modified according to insight gained in the meanwhile: (i) the onset of approximation validity there was 0.002 but due to recent analysis of pipe-inlet distortions [11] here it is shifted to $L_i = 0.003$; (ii) accordingly the initial velocity value

was 1.18, whereas now it is 1.389; (iii) consequently, convergence rate is now 1/72 vs. 1/78 there – in order to still obtain 98% of the property change by $L_f = 0.05$, as was required there.

Similarly, the momentum flux grows according to:

$$M(L) = \frac{4}{3} - \left(\frac{4}{3} - \underbrace{1.15}_{M_i}\right) \cdot e^{-\frac{L-0.003}{1/72}} \tag{31}$$

where the value of M_i is the momentum flux for a pipe of length $L_i = 0.003$ (at the onset of the valid range).

The curvature representative radius as:

$$R_{c,n}(L) = \frac{\sqrt{6.}}{12} - \left(\frac{\sqrt{6.}}{12} - \underbrace{0.355}_{R_{c,i}}\right) \cdot e^{-\frac{L-0.003}{1/72}} \tag{32}$$

This virtual origin's variation is described by the same form used above, giving:

$$\Delta X(L) = \underbrace{0.0537}_{\Delta X_{dev}} - \left(0.0537 - \underbrace{0.063}_{\Delta X_i}\right) \cdot e^{-\frac{L-0.003}{1/72}} \tag{33}$$

And finally the near-axis profile curvature:

$$S_1 = \begin{cases} \underbrace{-4}_{S_{1,dev}} - \left(-4 - \underbrace{-4}_{S_{1,i}}\right) e^{-\frac{L-\overbrace{0.018}^{L_i}}{\frac{1}{72}\frac{0.05-0.018}{0.05-0.003}}} \cong -4\left(1 - e^{-\frac{L-0.018}{1/106}}\right) & L > 0.018 \\ 0 & L \leqslant 0.018 \end{cases} \tag{34}$$

Note that for the last expression, the developing pipe flow solution [34] states that the profile curvature at the axis begins only beyond $L = 0.018$ and the convergence rate must therefore be adjusted in order to still obtain 98% of the development by $L_f = 0.05$.

With all these explicit approximations comprising A_0, which do not require any pre-knowledge of the arriving profile, the heat transfer at stagnation Nu_0 can be directly predicted. It is now explicitly given in nominal geometrical terms L and H as:

$$\frac{Nu_0(L,H)}{Re^{1/2}G(Pr)} = \sqrt{\frac{A_{0,uni}\left(R_{c,n}(L)\, e^{-\left(1+\frac{2S_1(L)H_0}{W\cdot w_{c,n}(L)}\right)\frac{H}{H_0}} + 8\sqrt{\sqrt{\frac{6}{5}}-1}\,(H+\Delta X(L)(1-e^{-H/H_0}))\right)^{-1}}{\frac{e^{-\left\{\frac{w^2_{c,n}(L)}{w^2_{c,dev}}\right\}\frac{w_{c,uni}}{w_{c,n}(L)}\frac{H}{H_0}}}{w_{c,n}(L)+4S_1(L)H} + \frac{32\left((H+\Delta X(L))\cdot\left(1-e^{-\left\{\frac{w^2_{c,n}(L)}{w^2_{c,dev}}\right\}\frac{w_{c,uni}}{w_{c,n}(L)}\frac{H}{H_0}}\right)\right)}{3M(L)}}} \tag{35}$$

with S_1, ΔX, M, $w_{c,n}$ and $R_{c,n}$ given above, and with the well-known constants $w_{c,uni} = 1$, $w_{c,dev} = 2$, $H_0 = 1/60$. Note the validity range of this approximate form is: $L \geq 0.003$, below which upstream inlet effects distort the issuing velocity profile; and $H \cdot Re = h \geq z_w$ (for which an empirically-based explicit form is given in Appendix B) below which the downstream stagnation pressure affects the issuing velocity profile (a feedback effect).

This explicit form for Nu_0 is not only convenient for design and optimization purposes, but also sheds light on the occurrence of maximal heat transfer, when the wall is located near the end of the potential core [24,35].

The suitability of these simplified model relations will be demonstrated through the predictions of simulations in the Results section.

2.3. Numerical

In the present work, numerical solutions of the Navier-Stokes and energy equations were obtained, providing detailed velocity and pressure fields of submerged impinging-jets over the range of $Re = 250–2000$. The numerical methods have been described in detail in a previous work [11], and are only given here briefly. While unsteady flow phenomena, such as jet-edge vortex generation, have been found even at moderate Reynolds numbers [36–38], it has been experimentally demonstrated that small scale jets can be maintained steady under controlled conditions up to $Re = 1400–2000$ [39,17]. Moreover, studying even an idealized model of a *steady* impinging jet can provide fundamental insights and a foundation for dealing with the unsteady aspects. The flow was simulated until a steady velocity field was observed and verified, i.e., doubling the simulated flow time resulted in velocity profile variation of less than 1%. Therefore, subsequent cases were solved using a steady-state solver, without perceivable convergence issues.

The numerical models in the present study were solved using the finite volume open-source CFD code OpenFOAM [40], where velocity-pressure coupling was dealt with using the SIMPLE algorithm with the convergence criteria set to residuals below 10^{-4} and 10^{-6} for the momentum and energy equations, respectively. The working fluid was water at 20° and was considered to be Newtonian with constant thermophysical properties.

The numerical models (Fig. 4a) consisted of four axisymmetric domain sizes, both spanning 8 nozzle diameters in the radial direction. In the axial directions they spanned 3, 6, 12 and 18 diameters. A horizontal inlet was positioned at the top of the domain, followed by a stationary wall in the same direction. The far boundary in the radial direction was of the inlet/outlet type, where the Neumann pressure condition is applied for outflow and the Dirichlet condition for velocity inflow. At the inlet, different realistic velocity profiles were imposed, which were previously obtained in a nozzle flow study [11] and are shown in Fig. 4b, including: (1) a uniform profile, denoted *uni*; (2) five partially developed profiles denoted *par1* to *par5*, corresponding to nozzle lengths of $L = l/Re = 0.0015$, 0.003, 0.006, 0.01 and 0.014, accordingly (where l is the nozzle length normalized by its diameter d); and (3) a parabolic profile, denoted *dev*.

Fig. 3 demonstrates the evolution of the velocity profile with flight distance H ($\equiv h/Re$), also showing the effective near-axis gradients, defined by c and R_c.

The numerical domain was meshed with quadratic cells of varying size. Consecutive refinements by cell-splitting were preformed across the entire axial span and from $r = 0$ to: $r = 6$, 3.5 and 1. A fourth local refinement was made around the inlet in order to accommodate the high gradients associated the uniform issuing profile. Additionally, adjacent to the impinged wall, 20 layers of thin cells with an inter-cell growth size of 1.034 were placed in order to capture the high velocity gradients in the stagnation boundary layer. The final working mesh consisted of 230,262 to 1,372,662 cells for $h = 3$ and $h = 18$, respectively. The present numerical methods were verified in the previous mentioned study, and results validated by comparison with current and previous experimental data (Figs. 5–7).

3. Results

The results section follows the order laid out in the methods. First, the simulated trends of A_0 and z_w are validated against those in the literature and extended to both partially-developed issuing profiles and longer-flights. Then the new relations proposed for intermediate jet flight and relaxation parameters ($w_{c,w}$ & R_c) are evaluated. Finally, the method laid out for finding the stagnation-point heat transfer Nu_0 is used to predict trends and find the maximum for any level of issuing profile development. Using the relations developed in the Method section, all predictions are

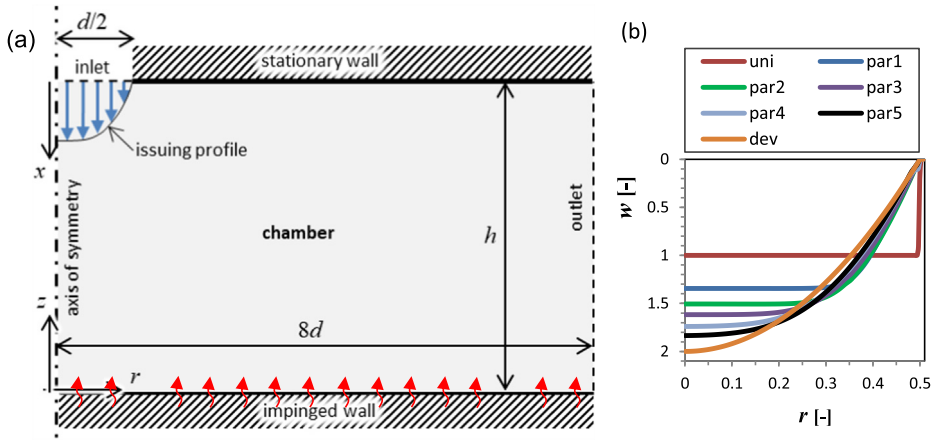

Fig. 4. The axisymmetric numerical model geometry (a) and all issuing profiles imposed at the inlet (b).

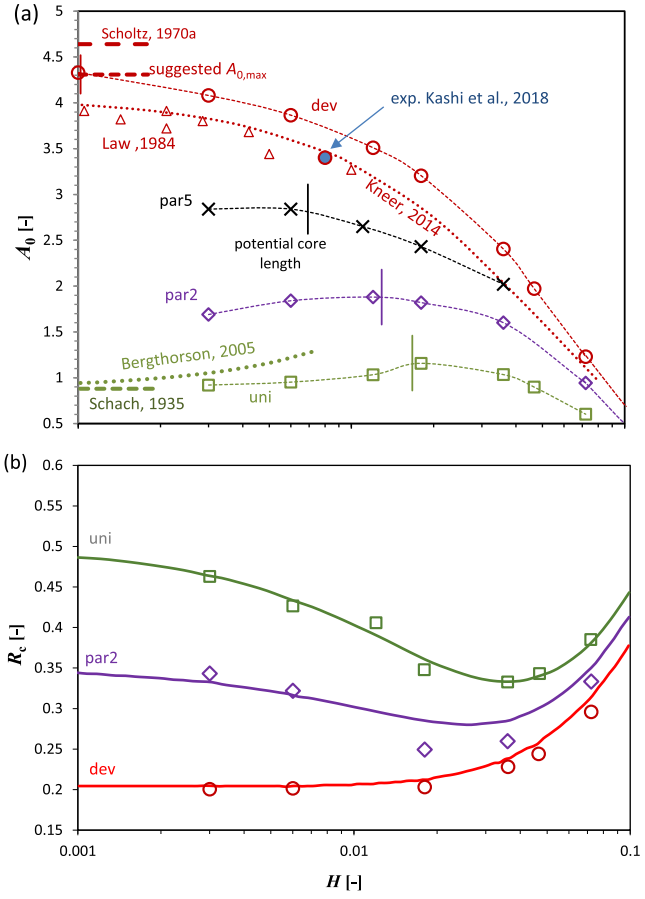

Fig. 5. The translation of flight characteristics to impingement behavior: (a) dependence of radial acceleration following impingement A_0, on issuing profile and flight distance H compared to current and previous data; (b) evolution of the jet-core during jet flight of three very different issuing profiles simulations (symbols) vs. prediction by Eq. (24) (solid lines); Note that the trend in (b) reflects that seen in (a) – supporting the derivation $A_0 \propto 1/R_c$.

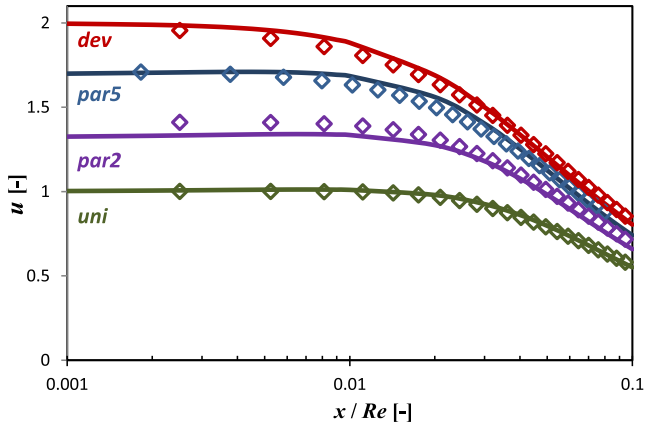

Fig. 6. Evolution of centerline velocity during flight for various issuing profiles, simulations (symbols) vs. prediction by Eq. (solid line); see Fig. 4 for the definitions of par2, par5 and dev.

evaluated by comparison to direct numerical simulations over a wide range of conditions ($0.003 \le L$, $0.002 \le H \le 0.072$, $250 \le Re \le 2{,}000$).

Proceeding to validate the trends found for A_0 by comparing the simulations to experimental and numerical data from the literature, it is seen that present simulations extend the available data also to intermediate, partially-developed cases as well as longer flights. As the figure shows, the trends from the literature are reproduced well, though values for a developed issuing profiles are slightly higher here – perhaps due to a closer examination of the stagnation point itself. For instance, slightly lower values are found in Kneer *et al.* [22] where an average in the vicinity of the stagnation point was extracted, similar to coarse-grid numerical solutions [28] and experimentally measured values, which are effectively averaged around the core. Moreover, in the light of the insight given in Eq. (18), a deeper look into Fig. 5 reveals two contributing factors to the ultimate decrease in A_0 with flight: the centerline velocity magnitude decay and the relaxation of the near-axis velocity gradients represented by R_c. This explains the opposing trends found in the literature: the near-nozzle increasing trend found by Bergthorson [1] for quasi-uniform profiles with a significant potential core vs the steadily decreasing trend for fully developed profiles [22]. For the former, the centerline velocity maintains its initial value, while the effective profile curvature increases as the potential core narrows and R_c decreases. By contrast, in the latter case opposing trends are encountered: while the centerline velocity decreases, R_c increases monotonously as the jet widens and the profile relaxes. This initial increase in A_0 for quasi-uniform or partially developed profiles (uni & par2 in Fig. 2) is eventually followed by a trend reversal and compliance with the far-flight decreasing trends. Moreover, it raises the question of the location of the maximum A_0 and consequently the maximum heat transfer, i.e., the optimal H for each level of pipe-flow development L, which will be addressed in the following.

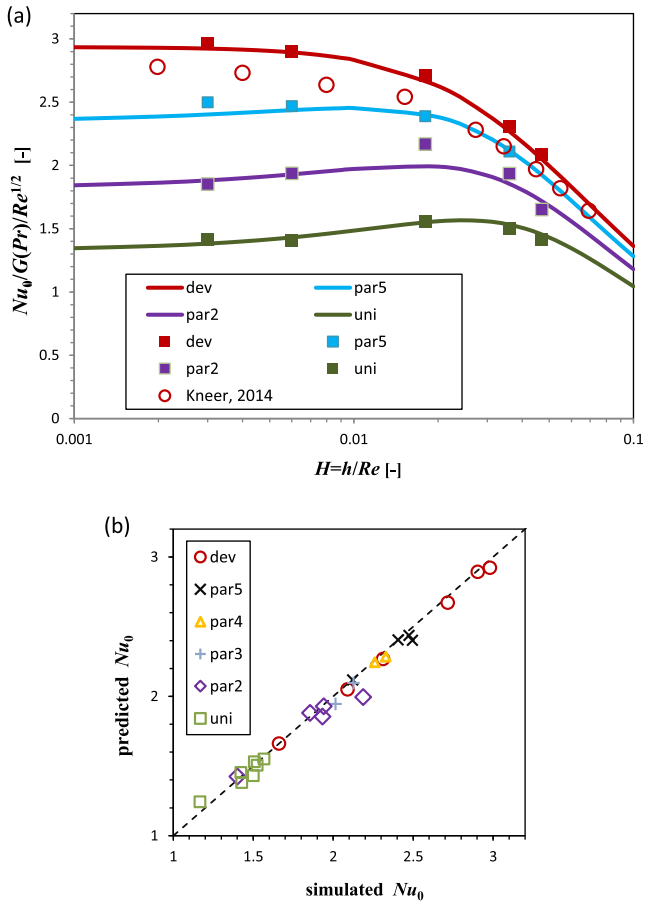

Fig. 7. Stagnation-point heat transfer vs issuing profile and flight distance: (a) trends prediction by the new model (solid lines) vs. present simulations (solid symbols) vs. previous fully-developed simulations (hollow symbols) [22] – Note that the latter data represents the average around the stagnation point, resulting in slightly lower values; (b) Evaluation of the prediction of the stagnation point heat transfer over a wide variety of arriving jets ($0.7 \le w_{c,w} \le 2$) under a wide variety of conditions ($250 \le Re \le 2{,}000$, $1 \le w_{c,n} \le 2$, $2 \le h \le 18$).

Beyond this insight, R_c and $w_{c,w}$ – the key elements of A_0, and ultimately of Nu_0, are evaluated in Fig. Figs. 5b and 6.

Both these figures verify the issuing values $R_{c,n}$ and $w_{c,n}$ (at $H = 0$) and the subsequent dependence of these parameters on H. Moreover, the graphs show that a simple transition between the two asymptotes is sufficient, subject to the correct scaling of the transition. This is the first time that such an analytically-based solution (which is smooth and fully differentiable in H) is presented for the centreline velocity w_c evolution during flight, thereby extending a previous empirically-based piecewise description [17]. Moreover, this is the first time that the importance of the jet-core curvature is identified and expressed through R_c and its newly found dependence on pipe-flow and subsequent jet flight.

Rather than returning now to prediction of A_0, the resulting heat transfer Nu_0 is shown explicitly in Fig. 7. Fig. 7a shows that the trends found in stagnation point heat transfer follow those previously seen in A_0 (Fig. 5), though they are somewhat damped per Eq. (6). Moreover, the present model clearly captures both the monotonously decreasing trend of a fully developed issuing profile and the trend reversal of partially developed ones. The quantitative evaluation of this new prediction is shown in Fig. 7b, where 83% of data are within 6% of predictions ($R^2 = 0.989$).

As the stagnation-point heat transfer trends in Fig. 7a show, partially developed profiles exhibit a maximum in H, around their potential core length. This raises the question of its exact location for optimal design within the geometrical constraints of nozzle-length and flight-distance. Moreover, the systematic analysis conducted here has revealed the cause of this maximum to be the maximal profile curvature. In other words, during the erosion of the potential core the jet-core curvature is increasing, while beyond the potential core relaxation decreases it. The location (H) of this maximum heat transfer is given for each issuing level of development (L) and compared to the potential core length found in a previous study [17], in Fig. 8.

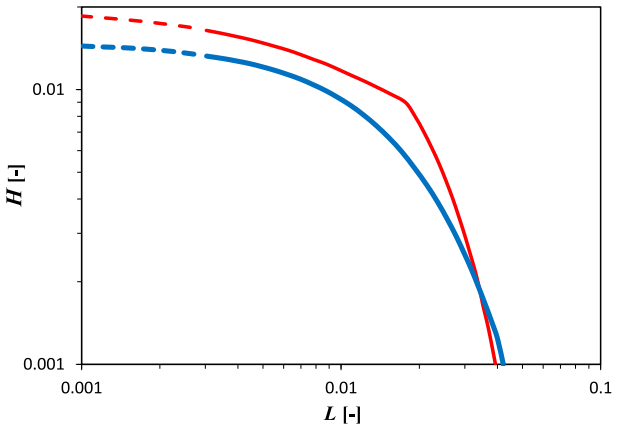

Fig. 8. The location of the maximum stagnation-point heat transfer in the geometrical domain (L, H) according to the new model vs. the location of the potential core (thin line from [17]). Dashed lines are extrapolations beyond the range of validity (valid for $L \ge 0.003$). Note the kink in the thick line, due to the regime change in the near-axis curvature in developing pipe flow being approximated by Eq. (34).

4. Conclusions

The present study addressed the need for a more comprehensive physically-based description of impinging jets and their heat transfer. Existing theory shows the direct connection between the stagnation-point radial acceleration A_0 and the heat transfer there Nu_0, but is limited to very specific cases (e.g., uniform flow). In most relevant cases the arrival profile, just prior to impingement, has been partially-developed in the preceding nozzle flow and partially-relaxed during preceding flight. A new theoretical analysis of stagnation flow was conducted, generally applicable in closed-form to a variety of arrival profiles, which result from the combination of a wide range of nozzle lengths, flight distances and flow rates ($6d \le L$, $2 \le h \le 18d$, $250 \le Re \le 2000$). All predictions and stages of development were verified against detailed numerical simulations.

Streamline-bending analysis shows the projection of dynamic pressure in the incoming jet on to the impinged wall, and led to the identification of the jet-core curvature as the key factor dictating A_0. Therein a new characteristic scale R_c defining the jet's core extent was found for evaluation of the global curvature of any profile. The newly found importance of this curvature, resolves the apparent contradicting trends found in the literature of the dependence of A_0 on flight distance. Moreover, it explains the occurrence of maximal heat transfer when the nozzle-to-plate spacing is set around the potential core length.

Building on the theoretical analysis, an explicit, yet universal, model for Nu_0 was developed in terms of nominal geometry and flow rate, rather than relying on the often-unknown arrival profile. Therein, this model pin-points the location of the maximal heat transfer during flight, for any partially-developed issuing profile. Moreover, owing to its simplicity, it permits this maximum to be easily sought out in design and optimization processes.

Finally, a new criterion for the onset of wall influence (at z_w) is proposed and shown to be consistent throughout all cases

considered. Furthermore, an existing wall-approach model was extended to include partially-developed profiles and longer flights. Then requiring its conformity to previous theory (Homann's stagnation flow) led to an explicit expression for the height of the stagnation zone (z_w). This parameter dictates the minimal nozzle-to-wall spacing, which still allows jet free-flight prior to impingement, thus permitting the underlying assumption of decoupling, which is foundational for present and previous heat transfer analysis.

A follow-up of this work, addressing the radial distribution of heat transfer and flow characteristics (boundary layer growth, wall shear, etc.) is currently underway.

Acknowledgement

This work was supported by the Israel Science Foundation [grant number 4112/17].

Appendix A. – The streamline bending analysis

To find the second relation required to obtain z_w and A_0 for each profile in a quantitative manner, streamline bending analysis was conducted. To quantify the streamline bending, occurring from arrival ($z = z_w$) to the the edge of the boundary layer ($z = \delta$), we seek out the extent of the radial "stretching" of the arriving profile, up to there. Alternatively, as all analysis is conducted at the wall radial coordinates, we in effect seek to tie it along its corresponding streamline to its origin at a height of z_w and a 'contracted" radial location R.

Beginning with a general analysis of the streamline bending during wall approach, therefore two opposing descriptions are available – Homann's near wall solution and the known behavior of jet flight, preceding the point of arrival. It is then noted that these two radial coordinates (R at z_w and r at δ) can be related by integrating the local slope over the full extent of the wall approach (from arrival and down to the boundary layer's edge):

$$[\mathrm{d}r]_{\delta} - \underbrace{[\mathrm{d}r]_{z_w}}_{\mathrm{d}R} = \int_{\delta}^{z_w} \frac{\mathrm{d}r}{\mathrm{d}z}\,\mathrm{d}z \tag{36}$$

We now seek to replace the small increment in the radial direction on the RHS with the characteristics of the arrival profile. First, within this domain it can be defined using the radial velocity ($\mathrm{d}r = u\ \mathrm{d}t$), giving

$$[\mathrm{d}r]_{z=z_w} - [\mathrm{d}r]_{z=\delta} = \frac{\mathrm{d}}{\mathrm{d}z}\left(\int_{\delta}^{z_w}\left(\frac{u}{r}r\,\mathrm{d}t\right)\mathrm{d}z\right) \tag{37}$$

In this steady flow, the axial velocity can assist to convert time- to space-dependency, according to $w = \mathrm{d}z/\mathrm{d}t$, while continuity is employed to begin to replace u with the dominant arrival velocity w:

$$[\mathrm{d}r]_{z=z_w} - [\mathrm{d}r]_{z=\delta} = \frac{\mathrm{d}}{\mathrm{d}z}\left(\int_{\delta}^{z_w}\left(-\frac{\partial w}{\partial z}r\frac{\mathrm{d}z}{w} - \frac{\partial u}{\partial r}r\frac{\mathrm{d}z}{w}\right)\mathrm{d}z\right) \tag{38}$$

Assuming Homann's solution holds, allows using his streamline relation, $r\,\mathrm{d}z = -2z\,\mathrm{d}r$, to obtain

$$\begin{aligned}[\mathrm{d}r]_{z=z_w} - [\mathrm{d}r]_{z=\delta} &= \frac{\mathrm{d}}{\mathrm{d}z}\left(\int_{\delta}^{z_w}\left(-\frac{\partial w}{\partial z}r\frac{\mathrm{d}z}{w} + 2\frac{\partial u}{\partial r}z\frac{\mathrm{d}r}{w}\right)\mathrm{d}z\right)\\ &= \frac{\mathrm{d}}{\mathrm{d}z}\left(\int_{\delta}^{z_w}\left(-\mathrm{d}w\frac{r}{w} + 2\mathrm{d}u\frac{z}{w}\right)\mathrm{d}z\right)\end{aligned} \tag{39}$$

As Homann's stagnation-flow solution is directionally decoupled as $w = w(z)$ and $u = u(r)$, the partial differentials can be written as complete differentials.

Now releasing the assumption of direction decoupling and allowing the incoming velocity to be non-uniform, i.e., fully distributed, leads to an expansion of the complete differentials to:

$$\begin{aligned}&[\mathrm{d}r]_{z=z_w} - [\mathrm{d}r]_{z=\delta}\\ &= \frac{\mathrm{d}}{\mathrm{d}z}\left(\int_{\delta}^{z_w}\left(\underbrace{-\frac{\partial w}{\partial z}\mathrm{d}z\frac{r}{w}}_{1} - \underbrace{\frac{\partial w}{\partial r}\mathrm{d}r\frac{r}{w}}_{2} + \underbrace{2\frac{\partial u}{\partial r}\mathrm{d}r\frac{z}{w}}_{3} + \underbrace{2\frac{\partial u}{\partial z}\mathrm{d}z\frac{z}{w}}_{4}\right)\mathrm{d}z\right)\end{aligned} \tag{40}$$

This expansion, which now involves mixed derivatives (i.e., directional coupling), is here taken as a first-order expansion of the decoupled form. In other words, this equation can be seen as a small deviation from Homann's solution, wherein his streamline relation still holds as long as the new terms "2″ & "4" are small. This requirement is complied with by staying near the axis, i.e., $r \ll 1$ (the exact limit will be found below): so that both the gradient and the coordinate in "2" tend to zero, while the gradient in term "4" is bound by small values at both ends of the wall approach (arrival and boundary layer edge) and being on the order of $\sim A_0 \cdot r/z_w$ must also converge to zero as the axis is approached. Employing again Homann's streamline relation and further simplification through the continuity equation gives:

$$[\mathrm{d}r]_{z=z_w} - [\mathrm{d}r]_{z=\delta} = \frac{\mathrm{d}}{\mathrm{d}z}\left(\int_{\delta}^{z_w}\left(\underbrace{-2\frac{u}{r}\mathrm{d}r\frac{z}{w}}_{1+3} - \underbrace{\frac{\partial w}{\partial r}\mathrm{d}r\frac{r}{w}}_{2} - \underbrace{4\frac{\partial u}{\partial z}\mathrm{d}r\frac{z^2}{rw}}_{4}\right)\mathrm{d}z\right) \tag{41}$$

Proceeding in the elimination of u from this expression several additional assumptions are still required. To this end, the derivative in term "4″, is expressed through the axis-symmetric vorticity relation $\omega \cong \tfrac{1}{2}(\partial u/\partial z - \partial w/\partial r)$, whereby the first term can be written as the fraction of vorticity passed over from the second, $\partial u/\partial z = C^2 \cdot \partial w/\partial r$. This characteristic ratio changes from $C = 0$ in developed pipe-type nozzle flow, through $C \propto 1/\sqrt{Re}$ during flight and increases to $C \sim 1$ within the stagnation zone – the flow enters with negligible radial velocity and exists with $u \sim 1$ over a distance of $z_w \sim 1$. In effect, Homann assumed irrotational flow outside the boundary layer, equivalent in the present analysis to $C = 1$, though here a characteristic value is sought on this order though not equal to 1, leading to

$$[\mathrm{d}r]_{z=z_w} - [\mathrm{d}r]_{z=\delta} = \frac{\mathrm{d}}{\mathrm{d}z}\left(\int_{\delta}^{z_w}\left(-\frac{2uz}{wr}\mathrm{d}r - \frac{\partial w}{\partial r}\frac{r}{w}\left\{1 + 4C^2\frac{z^2}{r^2}\right\}\mathrm{d}r\right)\mathrm{d}z\right) \tag{42}$$

when approaching the axis, the unity term in the curly brackets becomes negligible when $r \ll 2C \cdot z$. Now, preforming the integration over the height of the stagnation zone – i.e., from δ to z_w and the differentiation by z gives

$$\begin{aligned}[\mathrm{d}r]_{z=z_w} - [\mathrm{d}r]_{z=\delta} = &\left[\left(\underbrace{-\frac{2uz}{1'}}_{} - \underbrace{4C^2\frac{\mathrm{d}w}{\mathrm{d}r}\frac{z^2}{wr}}_{2'}\right)\mathrm{d}r\right]_{z=z_w}\\ &- \left[\left(\underbrace{-\frac{2uz}{3'}}_{} - \underbrace{4C^2\frac{\mathrm{d}w}{\mathrm{d}r}\frac{z^2}{wr}}_{4'}\right)\mathrm{d}r\right]_{z=\delta}.\end{aligned} \tag{43}$$

In this equation some terms on the RHS can clearly be neglected relative to the second term which is ≫1: (i) the first term contains the radial velocity under arrival flow conditions known to be very small – according to Schlichting's self-similar solution $u/(\partial w/\partial r) \sim O(1/Re)$, also confirmed for other profiles by present simulations; (ii) the third term is of order δ; (iii) the last term of order δ^2, leaving only

$$[\mathrm{d}r]_{z=\delta} = \left[\mathrm{d}r + \left(4C^2\frac{z^2}{r^2}\right)\frac{\mathrm{d}w}{\mathrm{d}r}\frac{r}{w}\mathrm{d}r\right]_{z=z_w}. \tag{44}$$

Multiplying both sides by r and integrating over the radial domain from the axis to the radial coordinate of the streamline, gives the relation between the streamline's ends, based on the shape of the arriving profile is:

$$r \equiv r|_{z=\delta} = \sqrt{r^2|_{z=z_w} + 8C^2 z_w^2 \ln\left(\frac{w(r)|_{z=z_w}}{w_w}\right)} = \sqrt{R^2 - 8C^2 z_w^2 \ln\left(\frac{w(R)}{w_w}\right)} \tag{45}$$

Note that as the LHS refers to the streamline's arrival at the boundary layer edge ($z = \delta$) at a radial position r, while the RHS denotes its origin at the stagnation zone height ($z = z_w$) at a contracted radial location conveniently defined by $R \le r$. The transition to a "jet flight" coordinate system (R,x) introduces a sign change in the last term, as $w(r,z) = -w(R,x)$.

Appendix B. – The axial wall approach

The new resolution of A_0 undertaken in this study also provides the opportunity to resolve the stagnation zone height (z_w) and generalize an existing wall approach model to all arrival profiles. The former, being the location of the onset of wall-influence (initial static pressure rise), will be shown to be the key characteristic scale for a general wall-approach description. To demonstrate the variability and trends of z_w values, data is shown from a wide range of present simulations in Fig. 9. As the figure shows, z_w decreases with an increase in level of profile development within the nozzle ($z_w \propto 1/L$), and increases with level of relaxation during flight ($z_w \propto H$). In the following both these influencing parameters are accounted for through the modification of an existing wall-approach model.

The values of z_w correspond to a criterion for transition from free-jet flight to stagnation flow. Despite several works dealing with this transition (Kostiuk *et al.* 1993; Bergthorson *et al.* 2005; Rohlfs *et al.* 2014a), only the latter suggested an objective criterion, though limited to the developed case only and concluding that $z_{w,dev} \cong 1$. Considering the primary effect of the wall – a static pressure build-up as the approaching flow decelerates, and considering this value reliable for the impingement of a purely parabolic profile, the value is seen to correspond with a criterion of $p(z_w) = 0.004 \cdot p_0 = 0.004\ ½\rho w_{c,w}^2$, i.e., a 0.4% static pressure rise. This value will be re-examined for consistency, once the analysis is complete.

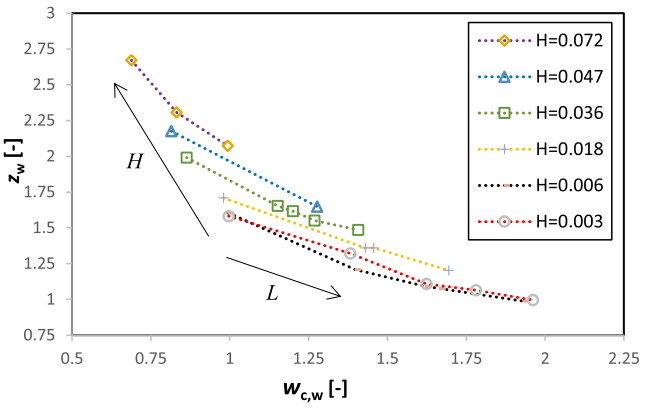

Fig 9. Stagnation zone height for submerged jets under various levels of pipe-flow development and flight relaxation.

Despite the importance of z_w and its significant variability, the only closed-form for wall-approach in the literature [1], was limited to short flights, weakly developed profiles and overlooked the importance of z_w. An earlier work showed a rather complex solution only for the fully developed case, which apparently followed an exponential decay towards the wall (see Fig. 6 in [30]). Here a combination of these is formulated into a new model, incorporating the exponential decay form as well as a normalized wall-approach coordinate (ζ) and corrections accounting for the deviations of the arrival profile from the uniform reference case. Thereby, extending this model beyond specific limiting cases to a wide range of possible profiles, occurring at longer flights and longer pipe-type nozzle flows, it formulated as

$$-\frac{w_c(z)}{w_w} = 1 - \exp\left(-4.605 \cdot \underbrace{\frac{z - 0.755/\overbrace{\left(Re^{1/2}w_w\right)}^{\approx\sqrt{ReA_0}}}{z_w}}_{\zeta=0\div1} \cdot \left[\frac{z_{w,uni}^2}{z_w^2}\frac{w_{w,uni}}{w_w}\right] \cdot \left\{\frac{w_n}{w_w}\right\}\right) \tag{46}$$

where the value 4.605, corresponds to 99% convergence to the arrival centerline velocity, and subscripts n and w indicate the two jet extremes – at the nozzle and upon onset of wall influence (at z_w), while "uni" refers to the reference case of an ideal uniform profile ($w_{n,uni}$, $z_{w,uni}$). Here, the expression for displacement thickness at the stagnation-point is further simplified by the approximation $A_0 \cong w_{c,w}^2$, derived above Fig. 2, which is justifiable at the high-Re conditions ($Re \ge 200$) where the displacement thickness only has a weak bias effect. Note that a more suitable normalization than that previously used [1] is employed – whereby ζ reduces from 1 to 0 as the wall is approached, in the limit of Re → ∞. Finally, modifications are employed which account for relaxation (a function of flight distance $H = h/Re$) through the term in curly brackets and also for issuing profile (a function of pipe length $L = l/Re$) through the one in square brackets. This new model is validated by comparison to multiple submerged jet simulations, including various levels of nozzle-flow development and longer flights in Fig. 10.

As Fig. 10 shows the previous closed-form model [1] is not suitable for more developed profiles and longer jet flights.

Now, requiring the wall approach's compliance with Homann's axial near-wall solution, ties it to the newly resolved parameter A_0. This interrelation may be intuitively understood as A_0 represent the inverse of the resistance to radial flow evacuation, while z_w represents the resistance to the flow approaching the wall. Indeed, it is seen that these two are inversely related: e.g., the purely parabolic case has the highest A_0 and the lowest z_w and vice-versa for the uniform case. This can be intuitively understood as more-developed arriving profiles, with axial velocity concentrated around the axis and reduced at the outer regions, have higher near-axis radial acceleration A_0. In other words, a convex profile permits easier radial evacuation, which in turn generates less back-pressure for the approach and consequently a lower z_w.

Beginning with Homann's near-wall solution, which states that the near-axis radial acceleration can be found from the axial deceleration, $\partial w/\partial z = -2A_0 = \text{const.}$, following continuity, gives:

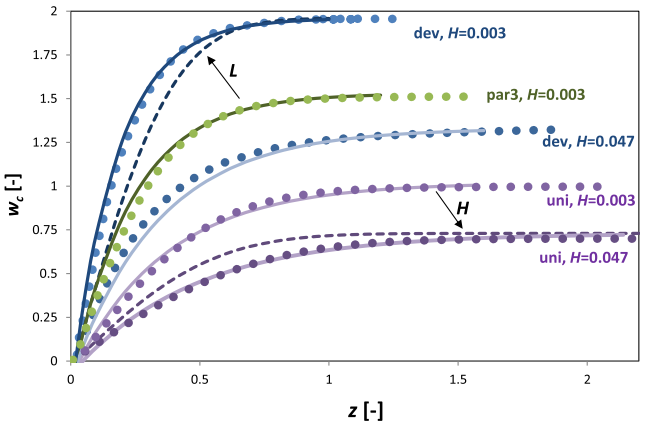

Fig. 10. The wall approach centerline velocity predictions (solid line) vs. simulations (dots), showing the extended range beyond a previous model (dashed line).

$$A_0 = -\frac{1}{2}\frac{\partial}{\partial z}\left(\frac{w_c(z)}{w_{c,w}}\right)_{z<<1} \tag{47}$$

Introducing the modified wall approach model, Eq. (46), into Homann's near-wall axial velocity Eq. (3), gives an explicit relation between z_w and A_0 for submerged jets:

$$A_0 \cong \frac{4.605}{2}\cdot\frac{z_{w,uni}^2\cdot w_{c,n}}{z_w^3\cdot w_{c,w}^2} \text{ or } z_w \cong \sqrt[3]{\frac{4.605}{2}\frac{z_{w,uni}^2}{A_0}\frac{w_{c,n}}{w_{c,w}^2}} \tag{48}$$

Introducing now the expression for A_0 from Eq. (18) the value of $z_{w,uni} = 1.56$, obtained from simulations according to the criterion discussed above $p(z = z_w) = 0.004p_0$, closes this model for z_w. Finally, the new explicit form of A_0 also leads to an explicit form of the stagnation zone height, through Eqs. (23) and (24):

$$z_w \cong \sqrt[3]{11.21\frac{R_c}{A_{0,uni}}\frac{w_{c,n}}{w_{c,w}^3}} \cdot \frac{w_{c,n}^{1/3}(L)\left(\frac{e^{-\left\{\frac{w_{c,n}^2(L)}{w_{c,dev}^2}\right\}\frac{w_{c,uni}}{w_{c,n}(L)}\frac{H}{H_0}}}{w_{c,n}(L)+4S_1(L)H}+\frac{32\left((H+\Delta X(L))\cdot\left(1-e^{-\left\{\frac{w_{c,n}^2(L)}{w_{c,dev}^2}\right\}\frac{w_{c,uni}}{w_{c,n}(L)}\frac{H}{H_0}}\right)\right)}{3M(L)}\right)}{=2.24\left(R_{c,n}(L)\,e^{-\left(1+\frac{12S_1(L)H_0}{5w_{c,n}(L)}\right)\frac{H}{H_0}}+8\sqrt{\sqrt{\frac{6}{5}}-1}\,(H+\Delta X(L)(1-e^{-H/H_0}))\right)^{-1/3}} \tag{49}$$

The evaluation of the prediction by this model by comparison to present simulation results is successful ($R^2 = 0.96$, N = 23).

References

[1] J.M. Bergthorson, K. Sone, T.W. Mattner, P.E. Dimotakis, D.G. Goodwin, D.I. Meiron, Impinging laminar jets at moderate Reynolds numbers and separation distances, Phys. Rev. E 72 (2005) 1–12, https://doi.org/10.1103/PhysRevE.72.066307.

[2] J.H. Lienhard, Liquid jet impingement, Annu. Rev. Heat Transf. (1995) 199–270.

[3] C.F. Ma, Q. Zheng, Local heat transfer and recovery factor with impinging free-surface jets of transformer oil, Int. J. Heat Mass Transf. 40 (1997) 4295–4308.

[4] M.D. Deshpande, M.P. Vaishnav, Analysis of endothelial lesions created using a submerged laminar jet, Biomed. Eng. I (1982) 107–109, https://doi.org/10.1016/B978-0-08-028826-0.50027-5.

[5] C.W. Visser, M.V. Gielen, Z. Hao, S. Le Gac, D. Lohse, C. Sun, Quantifying cell adhesion through impingement of a controlled microjet, Biophys. J. 108 (2015) 23–31, https://doi.org/10.1016/j.bpj.2014.10.071.

[6] C.V. Tu, D.H. Wood, Wall pressure and shear stress measurements beneath an impinging jet, Exp. Therm. Fluid Sci. 13 (1996) 364–373, https://doi.org/10.1016/S0894-1777(96)00093-3.

[7] G.T. Smedley, D.J. Phares, R.C. Flagan, Entrainment of fine particles from surfaces by gas jets impinging at normal incidence, Exp. Fluids. 26 (1999) 324–334, https://doi.org/10.1007/s003480050295.

[8] G. Ziskind, Particle resuspension from surfaces: revisited and re-evaluated, Rev. Chem. Eng. 22 (2006) 1–123.

[9] I.Z. Naqavi, J.C. Tyacke, P.G. Tucker, Direct numerical simulation of a wall jet: flow physics, J. Fluid Mech. 852 (2018) 507–542, https://doi.org/10.1017/jfm.2018.503.

[10] Y. Wang, R.E. Khayat, Impinging jet flow and hydraulic jump on a rotating disk, J. Fluid Mech. 839 (2018) 525–560, https://doi.org/10.1017/jfm.2018.43.

[11] B. Kashi, D.H. Haustein, Dependence of submerged jet heat transfer on nozzle length, Int. J. Heat Mass Trans. 121 (2018) 137–152.

[12] H. Schlichting, Boundary Layer Theory, 7th ed.,., Mcgraw-Hill Book Company, 1967.

[13] F. Homann, Der einfluss grosser zahigkeit bei der stromung um den zylinder und um die kugel, Z. Angew. Math. Mech. 16 (1936) 153–164.

[14] M.B. Glauert, The wall jet, J. Fluid Mech. 1 (1956) 625–643, https://doi.org/10.1017/S002211205600041X.

[15] E.N.C. Andrade, L.C. Tsien, The velocity-distribution in a liquid-into-liquid jet, Phys. Soc. 49 (1937) 381–391.

[16] A. Revuelta, A.L. Sánchez, A. Liñán, The virtual origin as a first-order correction for the far-field description of laminar jets, Phys. Fluids. 14 (2002) 1821–1824, https://doi.org/10.1063/1.1473650.

[17] B. Kashi, E. Weinberg, H.D. Haustein, Analytical re-examination of the submerged laminar jet's velocity evolution, Phys. Fluids. 30 (2018) 063604.

[18] D.J. Phares, G.T. Smedley, R.C. Flagan, The inviscid impingement of a jet with arbitrary velocity profile, Phys. Fluids. 12 (2000) 2046–2055, https://doi.org/10.1063/1.870450.

[19] L.W. Kostiuk, K.N.C. Bray, R.K. Cheng, Experimental study of premixed turbulent combustion in opposed streams. Part II -reacing flow field and extinction, Combust. Flame. 92 (1993) 396–409.

[20] W. Rohlfs, C. Ehrenpreis, H.D. Haustein, R. Kneer, Influence of viscous flow relaxation time on self-similarity in free-surface jet impingement, Int. J. Heat Mass Transf. 78 (2014) 435–446.

[21] W. Rohlfs, C. Ehrenpreis, H.D. Haustein, O. Garbrecht, R. Kneer, Influence of Local Flow Acceleration on the Heat Transfer of Submerged and Free-Surface Jet Impingement, Int. Heat Transf. Conf., Kyoto, Japan, 2014, pp. 1–14.

[22] R. Kneer, H.D. Haustein, C. Ehrenpreis, W. Rohlfs, Flow Structures and Heat Transfer in Submerged and Free Laminar Jets, IHTC15, Kyoto, Japan, 2014, pp. 1–21.

[23] L.W. Kostiuk, K.N.C. Bray, R.K. Cheng, Experimental study of premixed turbulent combustion in opposed streams. Part I - nonreacting flow field, Combust. Flame 92 (1993) 377–395, https://doi.org/10.1016/0010-2180(93)90150-2.

[24] H. Martin, Heat and mass transfer between impinging gas jets and solid surfaces, Adv. Heat Trans. 13 (1977) 1–60, https://doi.org/10.1145/2505515.2507827.

[25] C. Meola, A new correlation of nusselt number for impinging jets, Heat Transf. Eng. 30 (2009) 221–228, https://doi.org/10.1080/01457630802304311.

[26] B. Kashi, H.D. Haustein, Microscale sets a fundamental limit to heat transfer, Int. Comm. Heat Mass Trans. 104 (2019) 1–7.

[27] X. Liu, L.A. Gabour, J.H. Lienhard, Stagnation-point heat transfer during impingement of laminar liquid jets: analysis including surface tension, J. Heat Transf. 115 (1993) 99–106, https://doi.org/10.1115/1.2910677.

[28] H.S. Law, J.H. Masilyah, Mass transfer due to a confined laminar impinging axisymmetric jet, Ind. Eng. Chem. Fundam. 23 (1984) 446–454, https://doi.org/10.1021/i100016a012.

[29] M.T. Scholtz, O. Trass, Mass transfer in a nonuniform impinging jet - part II, AIChE (1970) 90–96.

[30] M.T. Scholtz, O. Trass, Mass transfer in a nonuniform impinging jet - part I, AIChE (1970) 82–90.

[31] A. Revuelta, A.L. Sánchez, A. Liñán, Confined swirling jets with large expansion ratios, J. Fluid Mech. 508 (2004) 89–98, https://doi.org/10.1017/S0022112004008948.

[32] F. Durst, S. Ray, B. Ünsal, O.A. Bayoumi, The development lengths of laminar pipe and channel flows, J. Fluids Eng. 127 (2005) 1154, https://doi.org/10.1115/1.2063088.

[33] H.D. Haustein, B. Kashi, Distortion of pipe-flow development by boundary layer growth and unconstrained inlet conditions, Phys. Fluids. 31 (2019), https://doi.org/10.1063/1.5091602.

[34] H.D. Haustein, R.S. Harnik, W. Rohlfs, A simple hydrodynamic model of a laminar free-surface jet in horizontal or vertical flight, Phys. Fluids. 29 (2017), https://doi.org/10.1063/1.4996771.

[35] K. Garrett, B.W. Webb, The effect of drainage configuration on heat transfer under an impinging liquid jet array, J. Heat Transf. 121 (1999) 803–810, https://doi.org/10.1115/1.2826069.

[36] M. Angioletti, R.M. Di Tommaso, E. Nino, G. Ruocco, Simultaneous visualization of flow field and evaluation of local heat transfer by transitional impinging jets, Int. J. Heat Mass Trans. 46 (2003) 1703–1713, https://doi.org/10.1016/S0017-9310(02)00479-9.

[37] Y.M. Chung, K.H. Luo, N.D. Sandham, Numerical study of momentum and heat transfer in unsteady impinging jets, Int. J. Heat Fluid Flow 23 (2002) 592–600, https://doi.org/10.1016/S0142-727X(02)00155-8.

[38] P. O'Neill, J. Soria, D. Honnery, The stability of low Reynolds number round jets, Exp. Fluids. 36 (2004) 473–483, https://doi.org/10.1007/s00348-003-0751-5.

[39] W. Rohlfs, J. Jorg, C. Ehrenpreis, M. Rietz, H.D. Haustein, R. Kneer, Flow Structures and Heat Transfer in Submerged and Free Laminar Jets, in: Proc. 1st Therm. Fluids Eng. Summer Conf., TFESC-1, New York City, USA, 2015, pp. 1–21.

[40] C. Greenshields, H. Weller, Implementation of semi-discrete, non-staggered central schemes in a colocated, polyhedral, finite volume framework, for high-speed viscous flows, Int. J. Numer. Methods Fluids. 63 (2010) 1–21.